REGULARITIES OF THE FORMATION OF THE MICROSTRUCTURE OF PHOSPHATE GLASSES DOPED WITH RARE-EARTH ELEMENTS

D. Grabco[1*], O. Shikimaka[1], M. Elisa[2], B. Sava[2], L. Boroica[3], E. Harea[1], C. Pyrtsac[1], A. Prisacaru[1], and Z. Danitsa[1]

[1]Institute of Applied Physics, Academy of Sciences of Moldova, 5 Academy str., Chisinau, MD-2028, Republic of Moldova, E-mail: grabco@phys.asm.md
[2]National Institute for Research and Development in Optoelectronics, Magurele-Bucharest, Romania
[3]National Institute for Lasers, Plasma, and Radiation Physics, Romania

(Received December 29, 2014)

Abstract

Intensive research into the various types of glassy materials (GMs) is being conducted due to their widespread application in many areas of modern engineering. However, despite the progress made in understanding the internal structure of GMs on the nanometer scale, the problem of the structure of long-range order on the nano/micro/macro scale remains very hypothetical. Therefore, we have studied the nano-microstructure of a large set of GMs belonging to the PhGs-R_2O_3 system, where *R* is rare earth metals (Pr, Nd, Sm, Eu, Gd, Dy, Ho, Er, Yb) and film/substrate structures ($P_2O_5 \cdot SiO_2$/SLG; $P_2O_5 \cdot SiO_2 \cdot Nd_2O_3$/SLG, SLG is soda-lime-glass).

We have shown that regardless of type of GMs, *common cluster-icosahedral-fractal regularities take place during the formation of GMs.* Close similarity between our results and the images of the literature data makes it possible to express an opinion of *the cluster-fractal structure* of GMs of different nature for both bulk glasses and film/substrate structures.

1. Introduction

Year by year, glassy materials (GMs) becoming more widely used in various areas of modern engineering as materials for photonics, optoelectronics, medicine and various branches of industry [1-6]. Wide application of GMs is also attributed to the relative simplicity of their production [7-9]. Today, intensive theoretical and experimental research into the various types of GMs (oxide glasses (OGs), metallic glasses (MGs), polymer glasses, etc.) is being conducted [4,10-25]. It is assumed that the glass structure consists of a strong covalent core (the so-called glass-matrix formed by strong covalent chemical bonds) and ion subsystems (the modifier elements) connected with the covalent skeleton by weak ionic chemical bonds. However, the real arrangement of atoms in the bulk structure of GMs is still poorly understood. It has been found [16,17] that the *atomic short-range order* (ASRO) exists in GMs: the nearest neighbor atoms and the second – nearest neighbors are arranged just as in a crystal with the same chemical composition. So, it has been established for GMs that a short-range order exists on a scale of <0.5 nm.

Short-range order is conditioned by the formation of *clusters*, in the center of which the atoms of "network formers" (*S,P,B,Pt*) surrounded by 9÷12 atoms of the "network modifiers" (*Na,Ca,Ni,Zr*) are located. Depending on the ratio of effective atomic radii, coordination numbers may slightly vary from cluster to cluster, providing a more efficient packing of atoms. However,

regardless of the particular type of ASRO, a *clustered short-range order* (CSRO), i.e., an orderly arrangement of several neighboring clusters relative to each other is present in glasses. For instance, in GMs, the CSRO is composed of about 70-80 atoms on a scale of ≈1.5 nm and is referred to as "*intermediate-range ordering*" or "*medium-range structural order*" (MRSO). Each cluster can be adjacent to ≈12 other clusters, which corresponds to an icosahedral packing. Voids between the clusters may, in turn, be filled with atoms or groups of solute atoms [2,13,14,18,24]. In addition, some models for MRSO have been proposed: a modified random network model [26]; a cluster bypass model [27]; a model of the salvation shell around the network-modifier atoms [28].

Thus, today, a variety of models exists to represent the internal structure of glasses with different compositions. However, all of them, in varying degrees, are probabilistic in nature because, on the one hand, the experimental methods used, despite their high accuracy, give an indirect idea about particular properties of the material tested; on the other hand, the molecular dynamics (MD) methods can create 3D structures with limited accuracy due to the complexity of multi-component GMs structure.

For this reason, despite the progress made in understanding the internal structure of GMs on the nanometer scale, the problem of the structure of long-range order (on the micro/macro scale) remains very hypothetical. Therefore, the aim of this study is to detect true images of the fine structure of GMs and reveal the principal regularities of formation of GMs.

For the first time, in our work, the real microstructure of a large set of OGs on the long-range scale has been demonstrated by direct experimental observations and, on this base, a *cluster-icosahedral-fractal mechanism of formation of GMs has been proposed.*

2. Experimental

Bulk phosphate glasses (PhGs) belonging to the $Li_2O \cdot BaO \cdot Al_2O_3 \cdot La_2O_3 \cdot P_2O_5 \cdot R_2O_3$ and $SiO_2 \cdot P_2O_5 \cdot R_2O_3$ systems, where *R* is rare earth metals (Pr, Nd, Sm, Eu, Gd, Dy, Ho, Er, Yb), which were used as doping elements (PhGs-R), were selected to solve the problems in this study. The concentrations of the elements in the PhGs-R samples were determined by inductively coupled plasma mass spectrometry (ICP-MS) and were ~2.5 wt % for the various rare-earth elements (REEs). The bulk PhGs were produced using an unconventional ("wet") procedure [8]. This approach comprises the following stages: (*1*) homogenization and water removal from the initial products at 100–120°C, drying at 180–200°C; (*2*) preliminary thermal treatment at 200–800°C prior to melting; (*3*) melting and refining at 1000–1200°C; (*4*) glass modeling; and (*5*) final annealing.

The film/substrate structures with the composition: (i) $P_2O_5 \cdot SiO_2$/SLG (soda-lime-glass) and (ii) $P_2O_5 \cdot SiO_2 \cdot Nd_2O_3$/SLG were prepared by the sol-gel method as described in [9]. The film thickness varied in a range of 2÷5 μm. The molar ratio of the final oxides for the first and second compositions was (i) P_2O_5/SiO_2=1/5; (ii) P_2O_5/SiO_2=1/5; $P_2O_5/NdCl_3$ =5.4; $SiO_2/NdCl_3$ =27 [29].

The surface morphology was investigated using the atomic force microscopy (AFM INTEGRA Prima) and light microscopy (LM) (Amplival and XJL-101 microscopes) in a regime of high contrast of reflected-light. The surface of the bulk samples was previously thoroughly polished with a silicon carbide powder to a mirror-like luster. A scanning electron microscope (Hitachi S-2600 N) equipped with an EDX analyzer was used for estimating the element distribution in the samples.

3. Results and discussion

Analysis of the surface morphology by the AFM method has shown that all the samples have a smooth surface without any cracks, pores or defects. The roughness (R_a) values were ~32 nm [9].

It has been found that the specific surface microstructure appeared by use of the LM with the subsequent computer rendering. Figure 1 shows the shape of the surface with original packages of the micron/submicron-scale aggregations recorded for two of bulk PhGs doped with Dy, Ho REEs. Similar images were obtained for other PhGs-R samples. It is significant that the particle bunches of a peculiar form are of different colors. At first glance, the images are chaotic and formless. However, a certain pattern becomes apparent on closer examination: the formation of specific figures close to a circle or an ellipse, which often overlap and thus distort their shape. Orientation and shape of the figures is somewhat different from each other in different parts of the surface.

For better visualitation of the above images, we selected two of samples (PhG-Dy and PhG-Nd) and marked various fragments with different dimension (Fig. 2, fragments 1-14) which show the formation of specific figure on the studied surface. Fragment 1 is one of the smallest that can be isolated at this magnification. Fragments 2-14 represent the structures that consecutively become more sophisticated, which consist of some (or much more) smalest fragments (blocks), and each of them in turn forms other more complex structure of a larger dimension. It is evident from Fig. 2 that the formation of these structures may be extended over large areas, in principle, closely covering the entire surface of the sample. The formation of these figures can be initiated from any place on the surface gradually attaching the figures lying in the neighborhood.

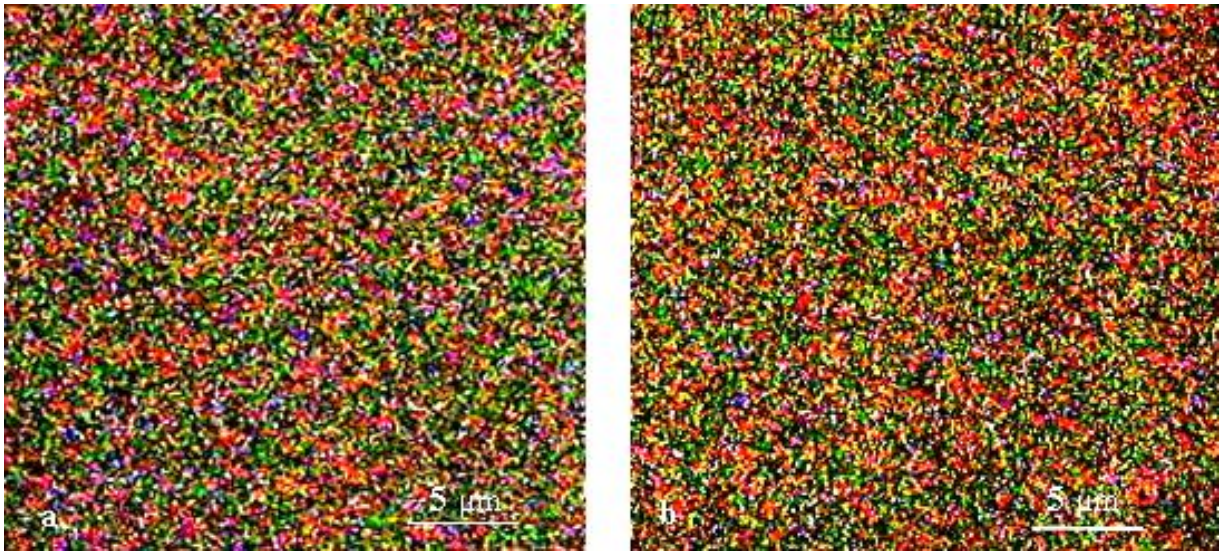

a) b)

Fig. 1. Images of the surfaces of PhGs doped with REEs detectable in the LM.
Samples: a) SP-Dy; b) SP-Ho.

The size of the blocks (fragments) forming specific patterns on the surface of OGs doped with REEs was estimated. For instance, the results for three glasses are shown in Table 1. Similar results were obtained for other PhGs-R. Table 1 shows that the values from a zone slightly vary

depending on the doping element. So, the glass containing Dy is composed of blocks smaller than in the glasses doped with Nd and Ho.

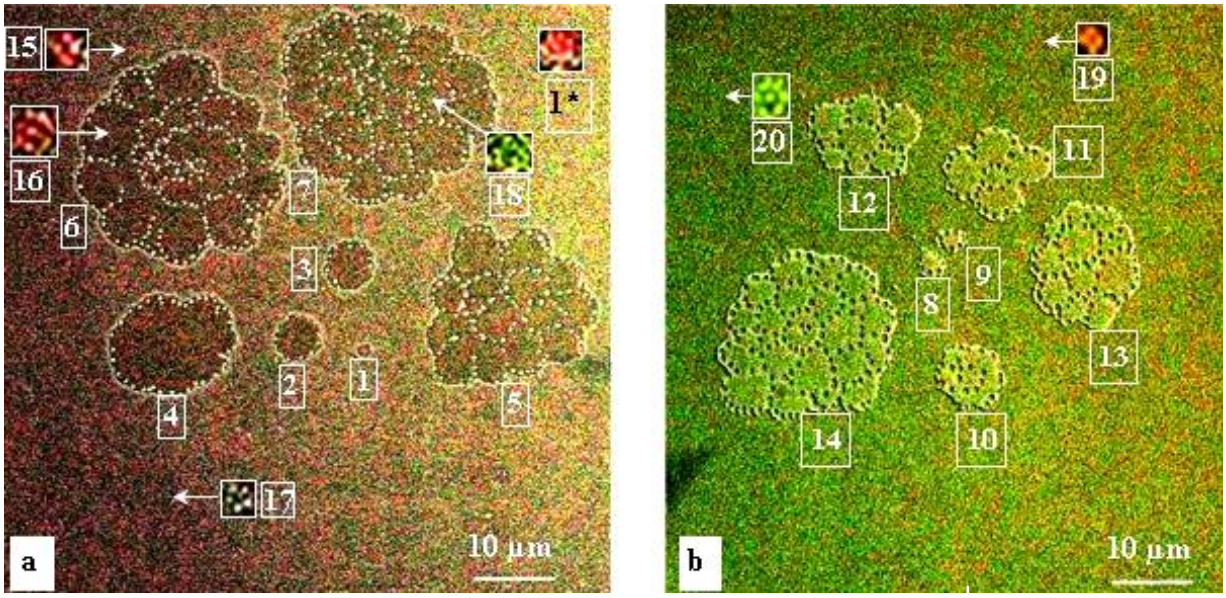

Fig. 2. Shape of the surfaces of two PhG-R glasses detectable in the LM: PhG-Dy (a); PhG-Nd (b). Zones of different dimension conditionally representing the fragments of different dimension (1-14) as the complexity of picrure. x800. Insert 1*- fragment 1 at higher magnification, x3600; inserts 15-20 show various fragments marked with arrows at higher magnification, x3600.

At the same time, the value of the most typical D_{mid} size does not significantly varies for different samples. Furthermore, there is a large range of block sizes: the largest is about 10 times larger than the smallest (cf. fragment 1 with 2, 3, 8-10, Fig. 2). Blocks 4-7 and 11-14 represent aggregates of the blocks of the 2, 3, 10 types.

Table 1. Approximate size of the smallest (D_{min}), middle (D_{mid}), and largest (D_{lar}) fragments characteristic of PhG-R visible at two different magnifications

Sample	Magnification x75			Magnification x1250		
	The smallest D_{min} value, µm	The middle characteristic D_{mid} value, µm	The largest D_{lar} value, µm	The smallest D_{min} value, µm	The middle characteristic D_{mid} value, µm	The largest D_{lar} value, µm
PhG-Nd	15	50÷65	140	1.0	8÷10	15
PhG-Dy	13	48÷60	130	0.7	3.5÷4	8
PhG-Ho	14	50÷70	150	0.7	4÷5	10

Note that the size of the detected blocks depends on the microscope magnification (on the microscope resolution); the higher the resolution of the LM, the smaller blocks can be detected on the surface (Fig. 3).

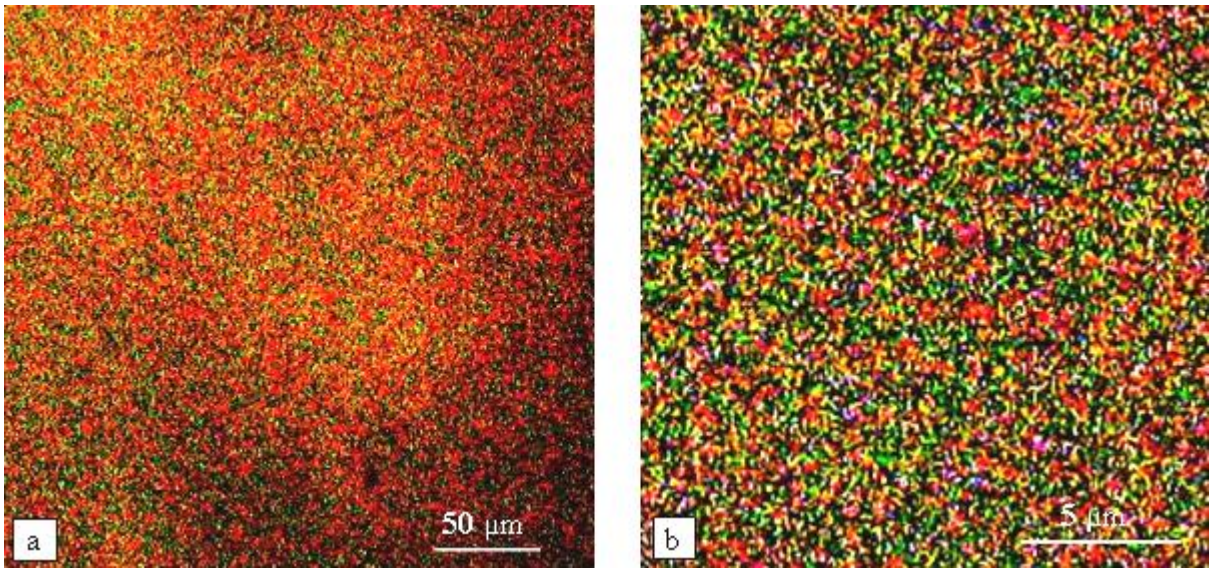

Fig. 3. Surface shape of the SP-Pr sample at two magnifications of the LM. (a) 20x and (b) 80x microscope objectives. The similarity of the microstructure shape of the samples at different scale levels is visible.

Thus, if the smallest blocks with a size of ~10 μm can be detected at the x75 magnification of the LM, the fragments on the order of 1 μm become apparent at x1250. An increase of the microscope resolution is accompanied by an increase in the number of particles of various colors indicating the identification of a finer structure of the samples. This alteration may also be visible under computer rendering. Fragment 1 (Fig. 2a) looks like a homogeneous structure at the x800 magnification, whereas at x3600 it consists of several petals (insert 1*, Fig. 2a). Similarly, inserts 15-20 represent the enlarged images of the figures indicated by arrows (Figs. 2a and 2b). On the other hand, one can distinguish the presence of microfragments of red and green color in fragments 2 and 3, whereas at the x75 magnification they appear as a homogeneous structure similar to fragment 1 in Fig. 2a.

Information presented above was confirmed and supplemented with experiments conducted for the composite structure of the ($P_2O_5 \cdot SiO_2$/SLG) and ($P_2O_5 \cdot SiO_2 \cdot Nd_2O_3$/SLG) film/substrate type using a scanning electron microscope equipped with an energy dispersion X-ray device (SEM-EDX). Figure 4 illustrates the elemental distribution of phosphorus (P) (Fig. 4a), silicon (Si) (Fig. 4b) and the joint distribution (P+Si) (Fig. 4c) in the $P_2O_5 \cdot SiO_2$ film. Fragments of round, oval, or subcircular forms of different size, closely similar to those in Figs. 1, 2 were clearly identified in all images of Fig. 4.

The images recorded for films of $P_2O_5 \cdot SiO_2 \cdot Nd_2O_3$ had a similar view. As an example, the illustration for the Si element distribution is presented in Fig. 5. For clarity, the image in Fig. 4a shows an aggregation of a large number of medium-sized units, which in turn is composed of even smaller units. A large aggregation can be extended in different directions as far as desired. The formation of aggregations, just as the shape in Fig. 4a, can be random from any point, increasing in different directions and tightly covering the entire surface. It is evident that the blocks are demarcated from each other by dark labyrinth-like (twisting) lines of an irregular form.

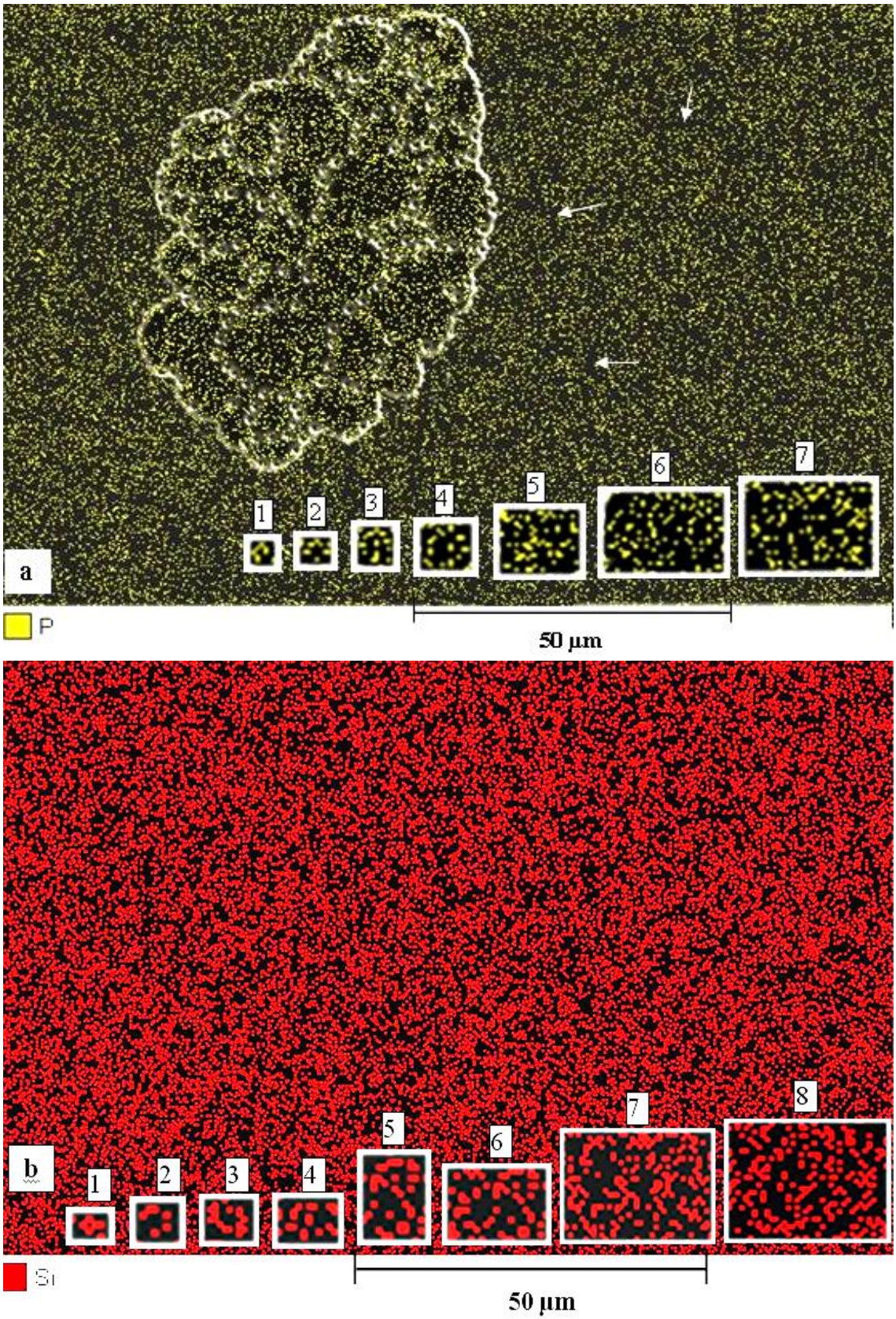

(continued)

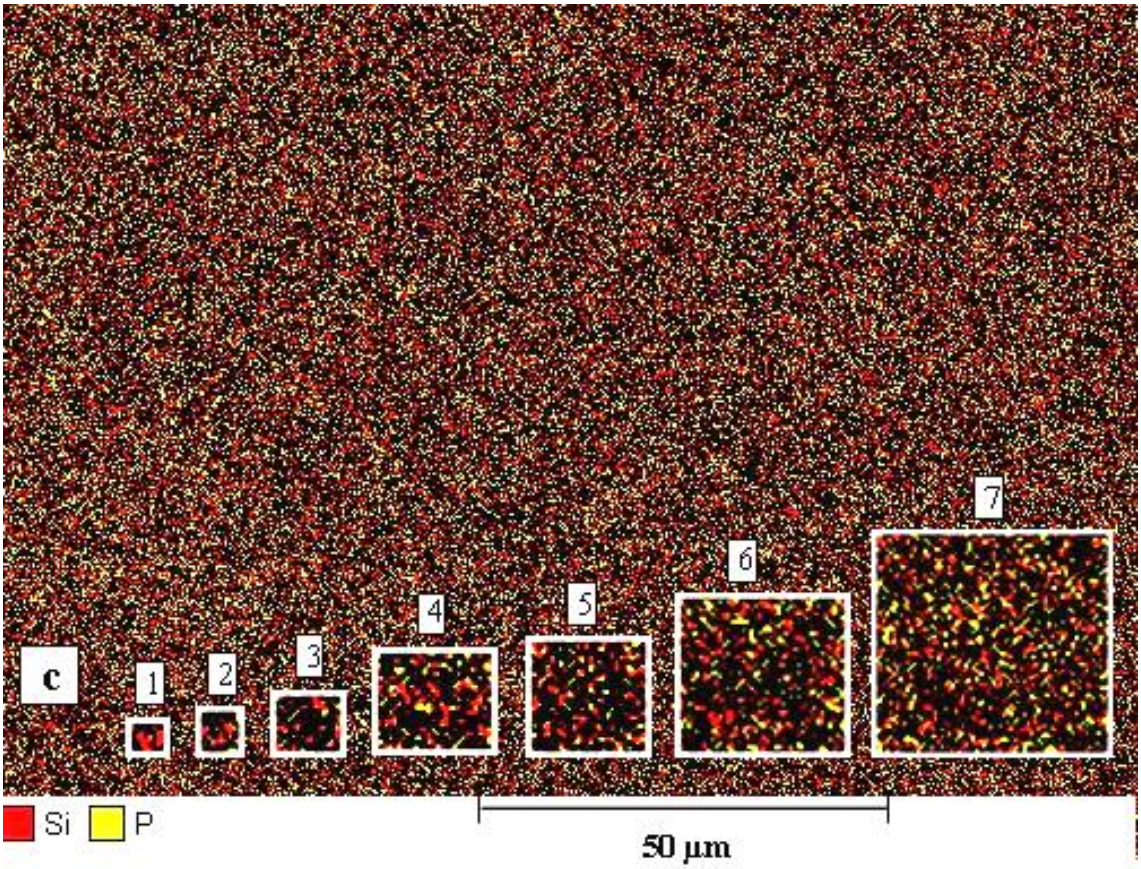

Fig. 4. SEM-EDX analysis of distribution of the P and Si elements in composite structure $P_2O_5 \cdot SiO_2$/SLG. (a) distribution of element P. In the center: an aggregation of a large number of medium-sized units conditionally marked on the surface; arrows indicate the dark labyrinth-like lines; (b) distribution of element Si. (c) distribution of elements (P+Si). (a-c) – Inserts 1–8: fragments of different complexity selected on the surface and presented at higher magnification, ~ x3600.

Note, that the fragmentary-block structure is characteristic not only of OGs. These patterns were obtained for GMs, gels, and polymers by many authors. So, Li et al. [30] showed the HRTEM image on the $Al_{89}La_6Ni_5$ GMs, which they characterized as "*a maze-like pattern with no discernable structure*". Using the confocal microscopy method, Lu et al. [23] demonstrated "*the fragmentary-block structure of the randomly-packed colloidal sediment"* prepared in a capillary with a centrifuge. Cluster formation and gelation were studied by Zhang et al. [22] in a colloidal model system and, the formation of the *fragmentary structure* of a gel was shown as well. The structural and dynamic characterization of the colloidal liquid-gel transition was presented by C.P. Royall with co-authors [25]; it was attributed to the formation of "*the specific icosahedral fragmentary structure*".

The dimension of the observed fragments depended on the analysis technique and ranged from 0.6÷12 nm to a few tens of micrometers [16-18, 25, 30, 31]. To compare these results with ours, we measured the fragment sizes in Figs. 4 and 5.

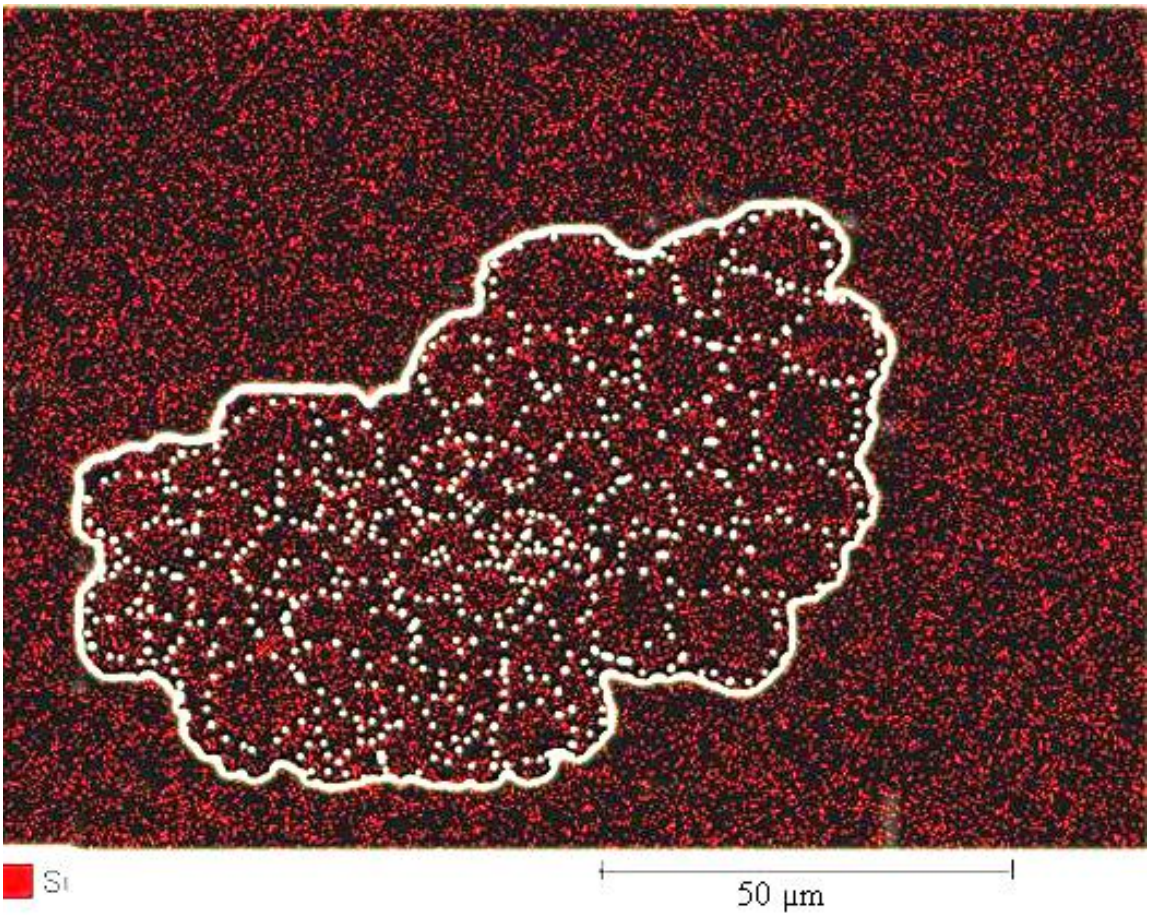

Fig. 5. SEM-EDX analysis of distribution of the Si element in composite structure $P_2O_5 \cdot SiO_2 \cdot Nd_2O_3$/SLG. In the center: an aggregation of a large number of medium-sized units conditionally marked on the surface.

The approximate sizes of fragments that are visible on the film surface for both investigated complex structures $P_2O_5 \cdot SiO_2$/SLG and $P_2O_5 \cdot SiO_2 \cdot Nd_2O_3$/SLG are presented in Table 2. The fragment sizes for both compositions of the film and for three estimation modes have almost the same value; that is, the discrepancies are within the counting errors. On average, the fragment that is minimally discernible at this magnification (x900) has a size of ~2 μm; the maximum size is on the order of 25 μm, and the most typical size is in a range of 8÷14 μm. Comparison of the values of Table 2 obtained for the films at x900 with the results of assessments of bulk glasses at magnifications x75 and x1250 (Table 1) shows good agreement of the data. Values for x900 (Table 2) are intermediate between the values for x75 and x1250 (Table 1). This fact suggest that the microstructure of the OGs obtained by different methods ("wet" melt-quenching method for bulk glasses and sol-gel method for film/substrate ones) is similar on the micron level. Moreover, by using confocal microscopy, similar images with closed dimensions were recorded for a hard-sphere-like colloidal suspension in a colloid-polymer mixture (ergodic liguid) (Figs. 1a-c, 2a-c in [25]) and a colloidal sediment prepared in a capillary with a centrifuge (Fig. 4a in [26]).

Table 2. Approximate size of the smallest (D_{min}), middle (D_{mid}), and the largest (D_{lar}) fragments characteristic of the $P_2O_5 \cdot SiO_2$/SLG and $P_2O_5 \cdot SiO_2 \cdot Nd_2O_3$/SLG film/substrate composite structures visible at the x900 magnification

Film sample	Defined elements	Magnification x900		
		The smallest fragment value, D_{min}, μm	The middle haracteristic fragment value, D_{mid}, μm	The largest fragment value, D_{lar}, μm
$P_2O_5 \cdot SiO_2$	P	2	10÷12	25
	Si	2	8÷11	23
	P+Si	1,5	10÷13	25
$P_2O_5 \cdot SiO_2 \cdot Nd_2O_3$	P	2	11÷14	26
	Si	2	10÷12	25
	P+Si	2	12÷14	26

At the bottom of each image in Figs. 4a – 4c, some inserts with images recorded at higher magnification (x3600) are placed to show the complexity of shapes that comprise the fragments. So, in the photographs that depict the distribution of phosphorus (Fig. 4a) and silicon (Fig. 4b) separately, inserts 1-4 show structures consisting of individual fragments similar to icosahedral-like clusters considered in [16,26]. They are referred to as "*icosahedral cluster packages*" (ICPs) and have a different number of petals: 4, 5, 6, 7, 8, 9, 12. Some cluster aggregations can be seen in inserts 5: three-clusters of phosphorus element ICPs and two-clusters of silicon element ICPs. The following inserts 6-8 are the multicluster formation of ICPs. Images with four, five, seven and more petals, like ICPs, became apparent after heat treatment in [32] of two co-authors (Elisa M. and Sava B.A.) of this paper.

Figure 4c shows the result of the combined (P+Si) elemental analysis. The general view of the pattern in all three images (4a -4c) is similar in both the fragment size and the shape inside the image. The difference is that in Fig.4c even in inserts 1-3 with single ICPs, both the phosphorous and silicon elements are present. Thus, the density of the particles in Fig. 4c almost doubled in comparison with Figs. 4a and 4b. A significant finding follows from analysis of the inserts presented on the Figs. 2, 4. Individual ICPs are combined together by the cluster-cluster or ICP-ICP interaction, thus forming larger agglomerations of a rounded shape (e.g., inserts 6-8 in Fig. 4b and inserts 4-7 in Fig. 4c).

Thus, in our research for a large set of GMs (bulk and films), the analogy of the structural formation of glasses in a wide range of scale: ASRO-MRSO-to-the-long-range order (*60-70 nm to $1 \cdot 10^4$ μm and more*) has been first shown experimentally on real samples. Comparison of pictures in Figs. 2 and 4 reveals regularity common for both the bulk and thin-film glasses, namely, the iteration of the pattern on a different scale, which is a property inherent in fractal structures. Moreover, this pattern can be traced by analyzing the works of other authors performed for different types of materials (MGs [17,30,31], OGs [14,16], gels [21,23,25,33]). Hence, this property is inherent in materials of different nature and different composition in a wide range of scales and demonstrates the *universality* of the phenomenon.

Confirmation of this is signified by the data presented in Table 3, which shows the results of analysis of the ICP content in different materials at varying the magnification. Thus, the number of ICPs in the D_{min} and D_{mid} fragments is 1÷2 and 2÷10, respectively, at very high magnifications (HRTEM method [16], [14]), whereas the number of ICPs at medium and low

magnifications (EDX SEM and LM methods) is 70÷900 and 450÷5000, respectively. It is noteworthy, that the number of ICPs is approximately the same for Si_3N_4-based ceramics and OG (NaLaGdSiO), despite a significant difference in magnification. We believe that the cause of this is the different size of the clusters and, consequently, the different size of the ICPs. According to [14,17,31,34], the cluster dimensions are ~0.5 and 5÷20 nm in MGs and OGs, respectively.

Table 3. Effect of magnification on the number of ICP in GMs

Samples	Magnification	Typical number of ICPs	
		in Dmin blocks	in Dmid blocks
Si3N4-based ceramics, HRTEM method [16]	x3500000	1÷2	2÷3
Oxide glass (NaLaGdSiO), HRTEM method [14]	x150000	1÷2	8÷10
Bulk PhG-Dy, AFM method	x40000	12	150
Bulk PhGs-R, LM method	x1250	70	450÷550
PhG-R film (here R:Nd), EDX SEM method	x960	166	850÷1000
Bulk PhGs-R, LM method	x75	900	3600÷5000

The following fact is significant: the formation of aggregations by icosahedral multicluster packaging is accompanied by a tendency to the structure rounding, and this tendency becomes more apparent with increasing aggregation size (see inserts in Fig. 4). Rounding usually occurs in a helical fashion or layer by layer. Figures 6a and 6b show three typical aggregates with circular layers on the PhG-Dy and PhG-Sm samples; idealized schemes for the aggregate formation are shown in Fig. 6c.

It should be noted that the real picture of the formation of ICP aggregates differs from the idealized concept scheme because the ICPs density in a glass solution is very high and a large number of the ICP aggregate nuclei is simultaneously formed during cooling [14]. These aggregates grow at the expense of the neighboring ICPs instantly occupying the entire volume and thereby interfering with each other to grow larger. In addition, by manipulating the temperature, stirring and cooling rate of the glass melt, it is possible to control the size of the ICP agglomerates formed in glasses. In turn, by controlling the size of the ICP aggregates, one can influence on changes in the optical, magnetic, mechanical, and other physical properties of the glass, which is very important for practical applications.

For clarity, the circles in Fig. 6c are of different shape and color because the chemical composition of layers in the glass structures can alternately change during the formation of ICP aggregates depending on the type and reactivity of the atoms, their concentration at the short-range atomic distance, the onset temperature of glass formation process, etc. As a consequence, one can get the impression of a certain *quasi-chaotic patterning* of the nano and microstructures of glasses.

Thus, the accumulated information about the properties of ICPs brings us to the idea of a *fractal structure* of GMs. The problem of the fractal structure of glasses has been studied intensively in recent years [32,35-40].

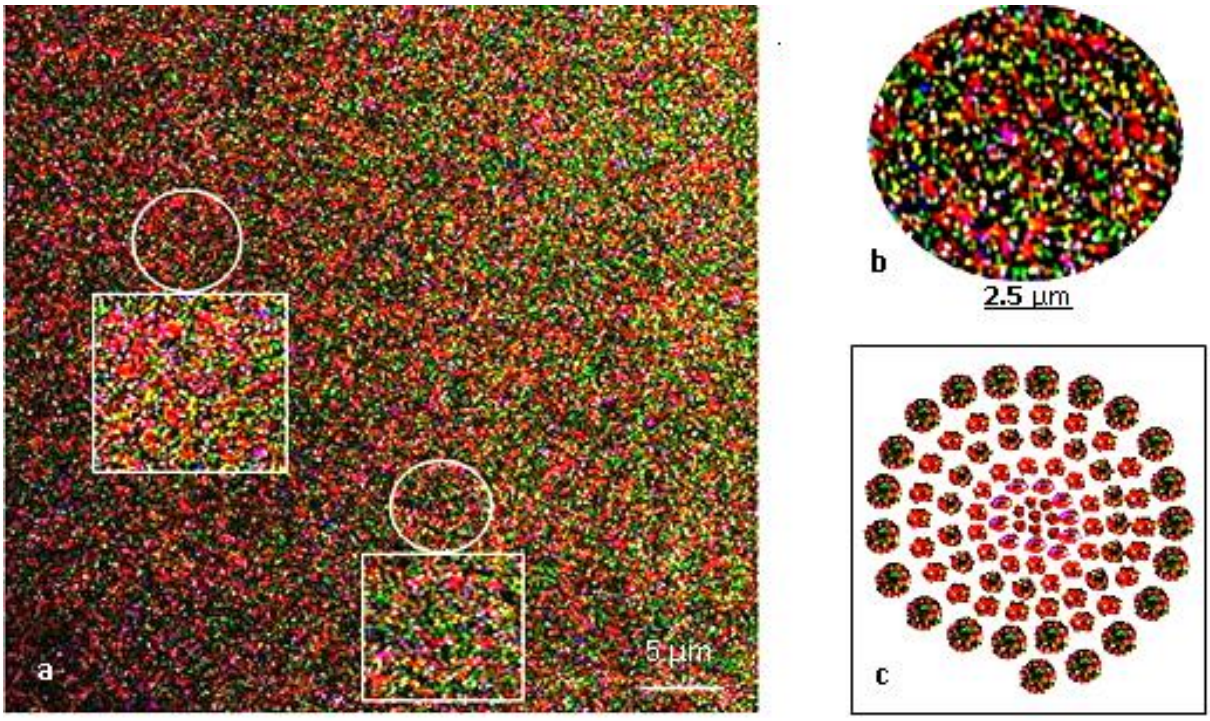

Fig. 6. Comparison of the real surface pattern of the PhG-R samples with idealized schemes of the ICP formation. (a) SLMR. Sample PhG-Dy; square inserts: scaled-up images of the round part; (b) Sample PhG-Sm, a part of surface like the (c) scheme, (c) Idealized scheme of the formation and evolution of ICPs.

It is known that *fractal* is a self-similar structure, shape or pattern, which is formed by repeating its parts on different scales [41]. A characteristic feature of a self-similar structure is that the shape of its parts is similar to the shape of the entire structure. The main properties of fractals are as follows: (i) fractals have a fine structure, i.e., contain arbitrarily small scales; (ii) fractals have some form of self-similarity allowing approximation; (iii) fractals are too irregular (*quasi-chaotic*) to be described in the traditional geometry language; (iv) fractals have a fractional Hausdorff-Besicovitch (H-B) dimension. Most of these properties, namely points (i)-(iii), have been reported in our work.

The results of other works can testify in favor of the (iv) point. Thus, Ma et al. [40] have theoretically shown that the power scaling in glasses gives characteristic parameters of H-B dimension of Df =2.31, which is less than the expected value of Df =3 for 3D solids. Other authors [37] calculated that the fractal dimension, interpreted as exponent n in the Avrami term, is 2.6, 2.4, and 2.2 at 539, 545 and 549 K, respectively. Avrami exponent n is responsible for the crystallization mechanism and related to the thermal stability of metallic glasses. Close similarity between the results presented in this study and the regularities typical of fractal structures makes it possible to express an opinion of *the cluster-fractal structure* of GMs of different nature for both bulk glasses and film/substrate structures. Moreover, this analogy is confirmed by the AFM pictures (Fig. 7), where the ICP configurations are detected at the nano/micro scale.

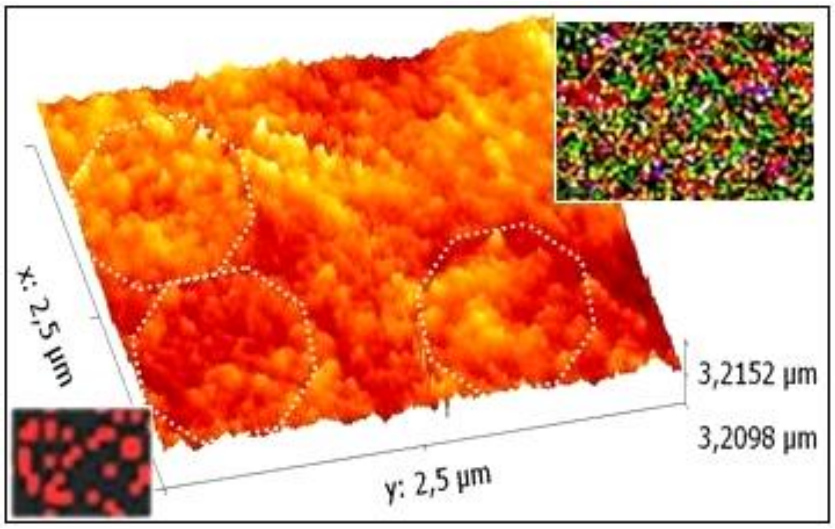

Fig. 7. Surface of PhG-Dy sample visualized by AFM method. Dotted hexagons mark three ICPs. The bottom insert: SEM-EDX image 5 from Fig. 4 b; The upper insert: LM image from Fig 6 a.

4. Conclusions

The currently available literature data show that the structure of non-crystalline solids is highly ordered *at the atomic level*. The laws of chemical bonding characteristic of crystalline materials act at this level. At the same time, by studying the real microstructure of a large set of the phosphate based glasses, we have revealed that GMs exhibit a specific random ordering at the *nano-micro-macro level* as a result of action of the specific ***cluster-icosahedral-fractal (CIF)*** *mechanism of structure formation.*

The discribed experimental data, which are in correlation with research results of many scientists for different types of GMs, have revealed *common cluster-icosahedral-fractal regularities in the mechanism of formation glassy compounds on the short-long-range scale regardless of type of GMs*, thereby opening a new fundamental principle for the interpretation of the structure formation process in amorphous materials.

This work was supported by the Moldovan–Romanian Intergovernmental Research Projects (project no. 10.820.05.21/RoF and project no. 13.820.05.20/RoF). The authors thank the National Center of Materials Science of Technical University of Moldova (grant RESC-MR-995) for AFM tests and Polytechnic University of Bucharest, the Department of Science and Engineering of Oxide Materials and Nanomaterials, România for SEM-EDX analyses.

References

[1] E. Axinte, Mat. and Design. **32**,1717 (2011).
[2] M. Karabulut, E. Metwalli, and R. K. J. Brow, J. Non-Cryst. Sol. **283,** 211 (2001).
[3] E. A. Abou Neel, D. M. Pickup, S. P. Valappil, R. J. Newport, and J. C. Knowles, J. Mater. Chem. **19(6)**, 690 (2009).

[4] S. Cai, W. J. Zhang, G. H. Xu, J. Y. Li, D. M. Wang, and W. J. Jiang, Non-Cryst. Sol. **355**, 273 (2009).
[5] O. V. Savvova, L. L. Bragina, and E. V. Babich, Nanosystem, Nanomaterials, Nanotechnologies. **8(4)**, 903 (2010).
[6] D. Carta, D. M. Pickup, J. C. Knowles, I. Ahmed, M. E. Smith, and R. J. Newport, J. Non-Cryst. Sol. **353**.1759 (2007).
[7] Werner Vogel, "*Glass Chemistry*". Springer-Verlag Berlin and Heidelberg GmbH & Co. K; 2nd revised edition (November 1994), ISBN 3-540-57572-3 .
[8] M. Elisa, C. Vasiliu, C. Grigorescu, B. A. Sava, A. Diaconu, H. J. Trodahl, and M. Dalley, Glass Technol.: Eur. J. Glass Sci. Technol. Part A. **48(5)**, 247 (2007).
[9] M. Elisa, I. C. Vasiliu, B. A. Sava, et al., Phys Chem Glasses: Eur J Glass Sci Technol, Part B. **51(6),** 309 (2010).
[10] U. Hoppe, J. Non-Cryst. Sol. **195**, 138-47 (1996).
[11] X. Yu, D. E. Day, G. J. Long, and R. K. Brow, J. Non-Cryst. Sol. **215**, 21 (1997).
[12] R. K. Brow, J. Non-Cryst. Sol. **263&264**, 1 (2000).
[13] J. Du, L. Kokou, J. L. Rygel, Y. Chen, C. G. Pantano, R. Woodman, and J. Belcher, J. Amer. Ceram. Soc. **84(8)**, 2393 (2011).
[14] H. Li, L. Li, M. Qian, D. M. Strachan, and Zh. Wang, Ceramic Transactions **170,** 69 (2005).
[15] G. Mountjoy, B. M. Al-Hasni, and C. Storey, J. Non-Cryst. Sol. **357(14),** 2522 (2011)
[16] T. Rouxel, J. Amer. Ceram. Soc. **90(10),** 3019 (2007).
[17] H. W. Sheng, W. Luo, F. Alamgir, J. Bai, and E. Ma, Nature **439,** 419 (2006).
[18] Y. Q. Cheng, and E. Ma, Progress in Mat. Sci. **56(4),** 379 (2011).
[19] A. Kartouzian, Nanoscale Research Letters **8**, 339 (2013) doi:10.1186/1556-276X-8-339.
[20] S. Ph. Salmon, and A. Zeidler, Phys. Chem. Chem. Phys. **15**, 15286 (2013).
[21] A. I. Campbell, V. J. Anderson, van J. S. Duijneveldt, and P. Barllet, Phys. Rev. Let. **94,** 208301 (2005).
[22] T. H. Zhang, J. Klok, R. H. Tromp, J. Groenewold, and W. K. Kegel, Soft Matter. **8,** 667 (2012).
[23] P. J. Lu, M. Shutman, E. Sloutskin, and A. V. Butenko, Optic Express. **25(21)**, 30755 (2013).
[24] B. Ruzicka, E. Zaccarelli, L. Zulian, R. Angelini, M. Sztucki, A. Moussaid, T. Narayanan, and F. Sciortino, Nature Mater. **10,** 56 (2011).
[25] C. P. Royall, S. R. Williams, T. Otsuka, and H. Tanaka, Nature Mater. **7,** 556 (2008).
[26] G. N. Greaves, J. Non-Cryst. Sol.**71**,203 (1985).
[27] M. D. Ingram, Phil. Mag. B. **60**,729 (1989).
[28] I. Farnan, P. J. Grandinetti, J. F. Stebnis, U. Werner, M. A. Eastman, and A. Pines, Nature. **358**, 35 (1992).
[29] D. Grabco, O. Shikimaka, M. Elisa, B. A. Sava, L. Boroica, E. Harea, C. Pirtac, A. Prisacaru, Feraru I., and Ursu D., Surf. Eng. & Appl. Electrochem. **48(5),** 430 (2012).
[30] G. O. Li, K. B. Borisenko, E. Ma, and D. Cockayne, Acta Mater. **57(3)**, 804 (2009).
[31] M. Chen, A. Inoue, W. Zhang, and T. Sakurai, Phys. Rev. Lett.96, 245502 (2006).
[32] M. Elisa, B. A. Sava, A. Volceanov, R. C. C. Monteiro, E. Alves, N. Franco, F. A. Costa Oliveira, H. Fernandes, and M. C. Ferro, J. Non-Cryst. Sol. **356**, 495 (2010).
[33] A. Malins, S. R. Williams, J. Eggers, H. Tanaka, and C. P. Royall, J. Non-Cryst. Sol. **357(2),** 760 (2011).
[34] P. H. Gaskell, and A. B. Mistry, Phil. Mag. **39,** 245 (1979).

[35] Yu. V. Barmin, I. L. Bataronov, A. V. Bondarev, and V. V. Posmet'yev, J. Phys: Condens. Matter. **20,** 114 (2008) doi:10.1088/0953-8984/20/11/114117.
[36] P. Charbonneau, J. Kurchan, G. Parisi, P. Urbani, and F. Zamponi, Nature Com. **5**, 3725 (2014) doi:10.1038/ncomms4725.
[37] K. Lad, M. Maaroof, K. G. Raval, and A. Pratap, Progr. Cryst. Growth & Charact. Mat. **45(1-2)**, 15 (2002) doi:10.1016/S0960-8974(02)00022-0.
[38] Meherun-Nessa, K. Shimakawa, A. Ganjoo, and J. Singh, J. Optoel. Adv. Mat. **2(2),**133 (2000).
[39] A. B. Golodenko, Semiconductors. **44(1)**, 84 (2010).
[40] D. Ma, A. D. Stoica, and X. L. Wang, Nature Mater. **8(1),** 30 (2009).
[41] Gordon Nigel, *Introducing fractal geometry*. Duxford, UK: Icon. p. 71. (2000). ISBN 978-1-84046-123-7.